in H_2O, each containing a D_2O capillary, was examined. The quantities K_{diss}, $F_{H_3O^+}$, and F_{HClO_4} were fit to the observed frequencies where

$$K_{diss} = \frac{[H_3O^+][ClO_4^-]}{[H_2O][HClO_4]} \quad (15)$$

$$F_{obsd} = \frac{3F_{H_3O^+}[H_3O^+] + 2F_{H_2O}[H_2O] + F_{HClO_4}[HClO_4]}{3[H_3O^+] + 2[H_2O] + [HClO_4]} \quad (16)$$

Using a program which obtains the best root-mean-square fit to the data, one obtains $F_{H_3O^+} = 9.333$ ppm. This may be compared with the earlier experimental value of Hood, Redlich, and Reilly, who obtained $F_{H_3O^+} = 9.17$ ppm.[6] Precise independent values for F_{HCLO_4} and K_{diss} could not be determined because these parameters were very strongly correlated. If both were varied maintaining the relation

$$K_{diss} = 1.79 - 0.105F_{HClO_4} \quad (17)$$

the rms (to be consistent with earlier use) deviation from the experimental data was affected little. The rms value improved slightly in the value of F_{HClO_4} went to high field (even above the frequency of water), but we believe that this is an artifact probably due to changes in the equilibrium constant and NMR properties of the solutions at high concentrations of perchloric acid. Thus, to fit the $F_H - F_D$ data we used $F_{H_2O} = 0$ and $F_{H_3O^+} = 9.333$ ppm.

With use of a multiparameter nonlinear least-squares fitting program to adjust the remaining parameters K_{iso}, $F_{D_3O^+}$, F_{HCLO_4}, F_{DClO_4}, and K_{diss}, all the data could be fit very well as shown in Table II. However, with so many free parameters, this is not surprising. Interactions between the parameters made it possible to vary pairs of them considerably without changing the rms deviation very much. The best fit rms deviation was 0.00178 ppm for $F_{D_3O^+} = 9.00$, $F_{HClO_4} = 5.70$, $F_{DClO_4} = 4.76$, $K_{diss} = 0.27$, the ratio of K_9 over $K_8 = 0.71$, and $K_{iso} = 1.60$.

All schemes, which we used for fitting the data, yielded a lower value for $F_{D_3O^+}$ than for $F_{H_3O^+}$. This would be an intrinsic isotope shift of 0.33 ppm (D_3O^+ relatively upfield relative to the water reference system). The magnitude of this shift is much larger than the values reported in Table I (±0.05 ppm); however, the broad shallow potential surfaces associated with the very strong hydrogen bonds to hydronium ion might cause this.[7] We are not sure that the difference between the fit values of F_{HClO_4} and F_{DClO_4} is significant and whether it indicates a similar large intrinsic isotope shift because of uncertainties in the fitting process as described above.

The reproducibility of our data is about ±0.2 Hz which leads to an uncertainty of ±0.1% in K_{iso}. Uncertainty of the value for the chemical shift difference between hydronium ion and water is one source of error in addition to the uncertainties in the fitting process. Also we do not know exact values for the equilibrium constants of eq 4-6. However, using the values of 2.93, 2.94, and 3.84 ppm yields a final result which is only different by 1% from the result obtained by using the statistical values of 3 and 4 ppm, since the effect of these changes in the two constants tends to cancel. Independent information about these constants might be obtained if measurements using this method were carried out at very high or low deuterium concentration. Then it should be possible to analyze the data with use of only the simple equilibria $D_3O^+ + HOD \rightleftharpoons HD_2O^+ + D_2O$ or $H_3O^+ + HOD \rightleftharpoons H_2DO^+ + H_2O$ without including the self-equilibrium constants in the analysis.

The present measurement of K_{iso} differs from previous measurements by specifically including the self-exchange equilibria and all of the interacting species in the analysis. Previous measurements by a variety of techniques rely on a generalized treatment of the data which results in a lower value of K_{iso} (1.41-1.5 ppm as summarized in Table III of ref 4). For example, in the most recent measurement, Heinzinger and Weston obtained $K_{iso} = 1.44$ ppm (D preferentially in water) by measuring the isotopic composition of the vapor over aqueous perchloric acid solutions at 13.5 °C.[4] Since their work was done with deuterium at natural abundance, they were actually measuring $H_3O^+ + HOD \rightleftharpoons H_2DO^+ + H_2O$ and *not* $(L)^{1/6}$.

The water-hydronium ion system is a complicated one and therefore has required a complicated analysis. However, cases where the molecules undergoing hydrogen-deuterium exchange have fewer exchangeable protons should be far simpler to analyze. Preliminary studies have indicated $F_H - F_D$ shifts in some of these systems, which are smaller than those reported in the present case; however, the use of very high field spectrometers should provide data of sufficient precision and accuracy for their useful analysis.

Acknowledgment. We would like to acknowledge support of this work by a grant from the Chemical Dynamics division of the National Science Foundation. We are also grateful for helpful conversations with Professor Max Wolfsberg. The high-field spectra were obtained at the Northeast Regional NSF-NMR Facility.

Registry No. $HClO_4$, 7601-90-3; deuterium, 7782-39-0.

(6) Hood, G. C.; Redlich, O.; Reilly, C. A. *J. Chem. Phys.* **1954**, *22*, 2067.
(7) A similar large intrinsic shift has been reported for the strongly hydrogen bonded proton in the enol of acetylacetone. (a) Altman, L. J.; Laungani, D.; Gunnursson, G.; Wennerstrom, H.; Forsen, S. *J. Am. Chem. Soc.* **1978**, *100*, 8264-66. (b) Chan, S. I.; Lin, L.; Clutter, D.; Dea, P. *Proc. Natl. Acad. Sci. U.S.A.* **1970**, *65*, 816.

NbO and TiO: Structural and Electronic Stability of Structures Derived from Rock Salt

Jeremy K. Burdett*[1] and Timothy Hughbanks

Contribution from the Department of Chemistry, The University of Chicago, Chicago, Illinois 60637. *Received October 11, 1983*

Abstract: The reasons underlying the structural stability of the four-connected NbO net and the "ordered defect" structure of stoichiometric TiO are presented. After showing the failure of an ionic model to account for the structures of these compounds, we show how the electronic structure of these materials explains their unique crystal structures. Analogies to M_6X_{12} clusters prove especially fruitful in this analysis. Both metal-metal bonding and metal-oxide π bonding are important in stabilizing these structures. The way in which vacancies enhance metal-metal bonding is discussed. Finally we conclude with a discussion of energetics and compare NbO with other four-connected nets.

In the field of structural chemistry those compounds that invariably hold the greatest fascination are those whose structures refuse to conform to our simple ideas of what they "ought to be". Prime examples of such compounds are the simple binary oxides

0002-7863/84/1506-3101$01.50/0

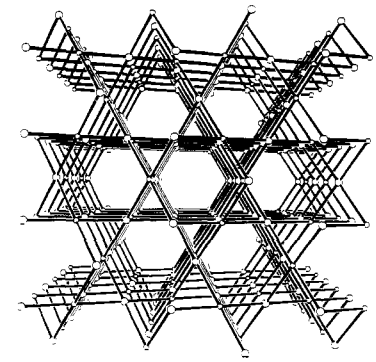

(a) NbO

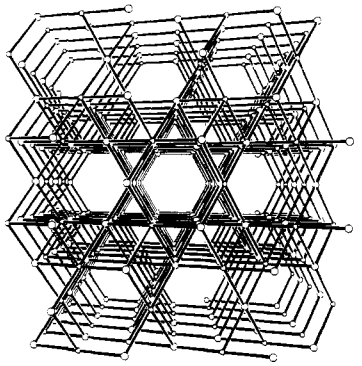

(b) TiO

Figure 1. NbO (a) and TiO (b) structures are projected perpendicular to the [111] direction of the parent rock-salt structure. Note that the proportion of sites with different coordination numbers can be clearly seen.

NbO and TiO. The NbO structure[2] is unique in having the arrangement indicated for the unit cell **1**, in which both Nb and

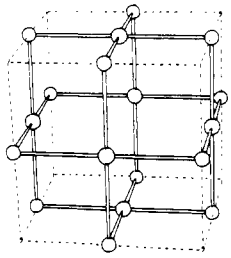

1

O occupy sites of square-planar coordination within a simple four-connected three-dimensional net. An alternative description is to say that NbO is an ordered defect rock-salt structure with one-fourth of the Nb and O atoms removed—in **1** they have been removed from the corners and center, respectively, of the indicated cube.

Stoichiometric TiO is also an ordered defect rock-salt structure[3] in which one-sixth of the metal and oxygen atoms are missing. The ordering of these defects may be related to the defect ordering in NbO by projection of the rock-salt structure on a (111) plane. The defects then show up as channels in NbO and TiO (Figure 1, parts a and b, respectively) which appear in lieu of missing –M–O–M–O– strings running along the (111) direction. Due to the close proximity of these channels in NbO, every atom in the structure is four-coordinate (square planar); in TiO only 20% are square planar and 80% are five-coordinate (square pyramidal). In both NbO and TiO each arrangement is its own "antistructure"; switching the places of the metals and oxygens leaves these compounds unchanged. A more conventional projection of TiO is on (100) planes of the rock-salt structure: planes of atoms at $z = 0$ and $z = {}^1/_2$ are shown for this centered monoclinic structure in **2**.

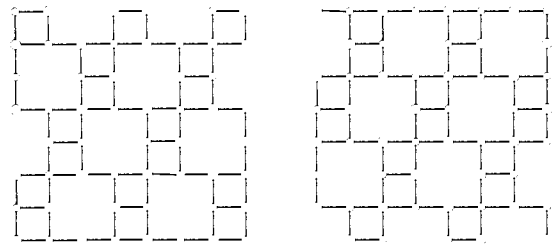

2

Why do these oxides have the structure that they have? Focusing on the local coordination of the atoms raises questions, not answers. Why should d^3 Nb (or d^2 Ti) be square planar? How do these structures stabilize square planar oxygen? Some simpler concepts familiar to solid-state chemists are also no help. Why should any such open structures be reasonable for these highly polar oxides? Madelung energies for NbO[4] and TiO are not only unfavorable with respect to rock salt but also with respect to "reasonable" alternatives with as many "defects" (see below). Attempts to rationalize these structures in terms of enhanced metal–metal bonding *as a result of a smaller lattice constant* are certainly unconvincing. Besides, there are fewer next nearest-neighbor metal atoms compared to the 12 in rock salt. In NbO, there are eight, and in TiO some have 9 and some 10 second nearest neighbors.

One avenue of approach in rationalizing these structures is particularly meritorious. Suggestions that NbO[5] and TiO[6] are just different ways of fusing M_6O_{12} units (as in **1**) fit in nicely with our theoretical picture. Perhaps because this point of view is difficult to explicitly account for in some phenomenological schemes,[7] there has been a tendency to ignore these suggestions.

Attempts to treat these systems as *actual* defect structures in which excess electrons are somehow trapped in the holes of the rock-salt parent structure are artificial in view of the very high concentration of such "defects". Also, the defects in NbO do not disappear upon application of pressure, and the TiO defect ordering is stable up to ~900 °C.[3a] Nonstoichiometry in TiO, at least on the O-rich side, is accommodated by intergrowth of TiO and $TiO_{1.25}$.[3a] The fact that such intergrowth can be observed (i.e., there are microdomains of both structural types) is indicative of the strong preference for a particular defect ordering in TiO. Also germane is the fact that the application of pressure causes a decrease in the vacancy concentration,[8] but with an *increase* in the lattice constant, perhaps indicating enhanced metal–metal bonding in the normal structure, if distance is the only guide. However, this provides no insight into the reasons behind the particular ordering of vacancies observed.

Failure of the Ionic Model

As the early transition-metal oxides are expected to be quite polar compounds, we might have anticipated that an ionic model

(1) Camille and Henry Dreyfus Teacher-Scholar.
(2) (a) Bowman, A. L.; Wallace, T. C.; Yarnell, J. L.; Wenzel, R. G. *Acta Crystallogr.* **1966**, *21*, 843. Brauer, G. *Z. Anorg. Allg. Chem.* **1941**, *248*, 1. Anderson, G.; Magneli, A. *Acta Chem. Scand.* **1957**, *11*, 1065. (b) Wells, A. F. "Structural Inorganic Chemistry", 4th ed.; Clarendon: Oxford, 1975.
(3) (a) Watanabe, D.; Terasaki, O.; Jotsons, A.; Castles, J. R. *J. Phys. Soc. Jpn.* **1968**, *25*, 292; "The Chemistry of Extended Defects in Non-Metallic Solids", North-Holland: Amsterdam, 1970. Watanabe, D.; Castles, J. R.; Jotsons, A.; Malin, A. S. *Acta Crystallogr.* **1967**, *23*, 307. (b) Hilti, E. *Naturwissenschaften* **1968**, *55*, 130.
(4) Hoppe, R. *Z. Anorg. Allg. Chem.* **1956**, *283*, 196.
(5) Schäfer, H.; von Schnering, H. G. *Angew. Chem.* **1964**, 833.
(6) Simon, A. *Angew. Chem.* **1981**, *93*, 23; *Angew. Chem., Int. Ed. Engl.* **1981**, *20*, 1.
(7) Goodenough, J. B. *Prog. Solid State Chem.* **1971**, *5*, 145–399.
(8) Banus, M. D. *Mater. Res. Bull.* **1968**, *3*, 723.

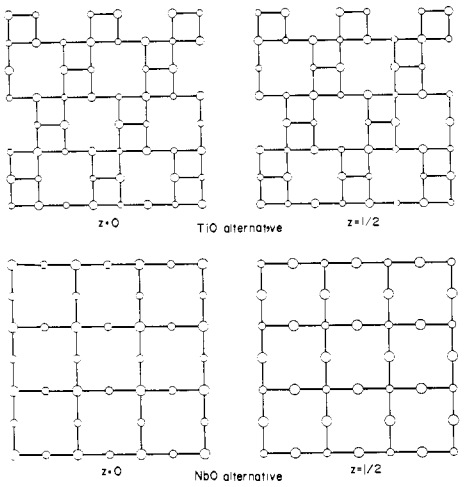

Figure 2. TiO alternative structure (a) and the NbO alternative structure (b) are projected on (100) planes of the parent rock-salt structure.

Table I. Madelung Constants for Various Monoxide Candidates

structure[a]	A_{R_0}	density, formula units/R_0^3
NaCl	1.7476	0.5
NbO	1.5043	0.375
TiO	1.5762	0.416
alternative NbO	1.6219	0.375
alternative TiO	1.6759	0.416
sphalerite	1.6381	0.325
PdO[b]	1.6102	0.334

[a] In each structure, R_0 = M–O remains fixed. [b] The Pd–O–Pd angle in PdO was taken as 98°.

would provide some insight into the structure of these systems. However, a little thought soon makes it clear that the presence of defects in a rock-salt structure as described for TiO and NbO above cannot be explained on simple Coulombic grounds. The more densely packed rock-salt structure will always be more stable per formula unit than the more open NbO and TiO structures. It has been argued that the formation of defects and concomitant density decrease would be compensated by a shrinking lattice constant (i.e., M–O distance) thereby recovering the "lost" Madelung energy of defect formation.[7] While we find such arguments unconvincing, they are irrelevant for reasons we now discuss.

If we restrict ourselves to the experimentally observed vacancy concentrations in TiO (16.7%) and NbO (25%), we might pursue the more modest goal of understanding the optimal (i.e., experimental) arrangement of these defects within the NaCl structure. The ionic model fails even in this task. This can be seen by constructing a defect pattern with a more favorable Madelung energy. One way to accomplish this is to shift the metal and oxygen vacancy sublattices of the *actual structures* so that metal vacancies are adjacent to oxygen vacancies. Alternative structures for TiO and NbO are indicated in Figure 2. These structures may be viewed as rock-salt structures from which columns of atoms have been removed along the (001) direction. In the NbO alternative one-fourth of such columns are removed; in the TiO alternative one-sixth of the columns are removed. We may think of vacancies as having effective charges via a "hole" formalism. Therefore structures that have vacancies of opposite effective charge less widely separated would be more favored in an ionic model. We have performed Madelung calculations[9a] on various structures including TiO, NbO, and the alternative structures above. The results of these calculations are given in Table I. As Table I indicates, the alternative structures have much more

(9) (a) A Born repulsion term was not included in these calculations. (b) Similar results are found when the ionic model is used to order vacancies in $Sc_{0.80}S$; see: Franzen, H. F.; Merrick, J. A. *J. Solid State Chem.* **1980**, *33*, 371.

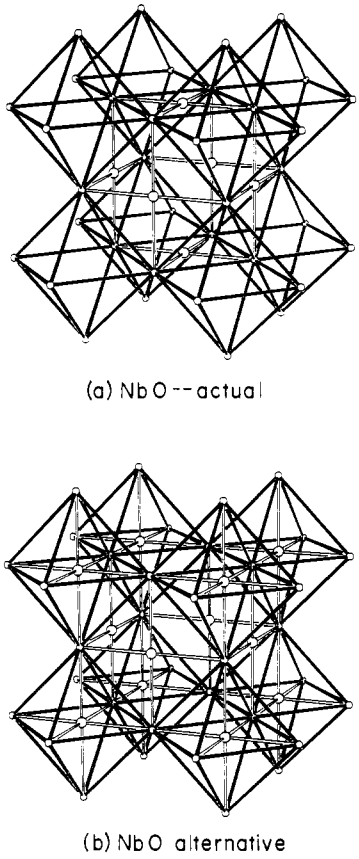

Figure 3. "Interstitial" locations of oxides in the cuboctahedral niobium net are shown: (a) the NbO structure in which oxides occupy square-planar sites only, (b) the NbO alternative in which octahedral interstices are filled in favor of one-third of the square-planar interstices.

favorable Madelung energies. In fact, of all the structures listed, NbO and TiO have the smallest Madelung constants—considerably smaller than even the open sphalerite and PdO structures.

The alternative NbO and TiO structures serve as particularly interesting controls for investigating the factors stabilizing the actual structures; not only do the alternatives have the same densities (by construction), but the metal sublattice is identical in the actual structures and their respective alternatives. This fact is illustrated for NbO and its alternative in Figure 3. NbO may be viewed as a cuboctahedral Nb net into which oxygen atoms are placed in all the square-planar interstices. The NbO alternative structure we have considered is obtained from NbO by moving one-third of the oxide ions (those in (001) planes) to octahedral interstices of the cuboctahedral Nb net. If M–M bonding is postulated as the factor that stabilizes the "defective" NbO and TiO structures, then the increased M–M bonding must be more than a result of a shrinking lattice constant in the defect structure since alternative structures with the same density and metal sublattice can be constructed. We intend to show that a careful examination of the *orbitals* involved in metal–metal bonding is necessary.

In any case, we have seen that the ionic model fails completely to describe the NbO or TiO structures.[9b] In one sense the observed structures are as bad as can be imagined: the metal and oxygen defects are as widely separated as possible for a given defect concentration. The ionic model predicts a substantial energetic preference for the alternative NbO and TiO structures. Per formula unit, the TiO and NbO alternatives are favored by $0.69q^2$ and $0.80q^2$ eV relative to the respective actual structures, where q is the magnitude of the charge assigned to the ions in Madelung calculations. (The Ti–O and Nb–O distances are assumed to be 2.08 and 2.11 Å in actual and alternative structures.)

Our strategy in this paper will be to seek an understanding of the factors that are responsible for the stabilization of the NbO

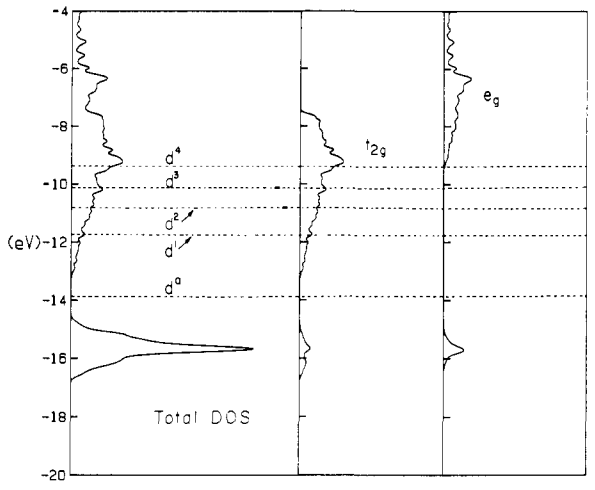

Figure 4. Density of states (DOS) curves for TiO in the rock-salt structure. The total DOS and the Ti d t_{2g} and e_g contributions are indicated. Lines indicating d-electron occupancies are given; for TiO the Fermi level would be at the d^2 line.

and TiO structures by analyzing the electronic structure of these compounds. In this analysis, we will entirely dispense with explicit considerations of the "Madelung" part of the energy of these systems. We do this with the full knowledge that this ignores a very significant contribution to the *overall* cohesive energies for these crystals since the structure-determining part of the crystal energy clearly lies outside the "ionic" contribution. This should not be seen as particularly disturbing in view of the fact that in a rigorous theoretical treatment there is no unambiguous way to identify "ionic" and "covalent" parts of the cohesive energy.

Orbitals for Rock-Salt Compounds

We begin with a description of bonding appropriate for fairly polar rock-salt compounds. As a zeroth order approximation, one may consider nearest neighbor σ bonding only. Since each atom is octahedrally coordinated by six atoms of the opposite variety, both M and X atoms may use $a_{1g}(s)$, $t_{1u}(p_x,p_y,p_z)$, and $e_g(d_{z^2},d_{x^2-y^2})$ orbitals (if available) for σ bonding to nearest neighbor atoms. Thus, for transition-metal systems, we are left with the $t_{2g}(xy,xz,yz)$ orbitals as nonbonding orbitals with respect to M–X σ bonding. Therefore, we might expect that the rock-salt structure would be "viable" for transition-metal oxides for d electron counts up to d^6 (low spin) since no M–O σ^* orbitals would be occupied for such electron counts. **3** illustrates these considerations.

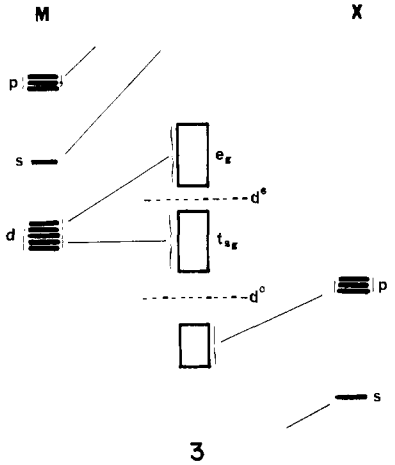

3

Of course, our discussion to this point simply mirrors one's expectations for low-spin molecular complexes. If we allow the next nearest neighbor metal atoms to interact, the t_{2g} orbitals may mix to form bands that will have metal–metal bonding character at the bottom and be metal–metal antibonding at the top of the band. This is the source of the width in the t_{2g} block in **3**. A detailed calculation on TiO (here assumed to adopt the NaCl structure) confirms the qualitative features implied in **3**. In Figure 4 we show the density of states (DOS) curves for rock-salt TiO as well as the t_{2g} and e_g contributions in the second and third panels, respectively. The lower sharp peak is from the oxygen p orbitals; the levels above −14 eV are primarily of d character. The shape of the DOS curve is characteristic, particularly just above the bottom of the d band.

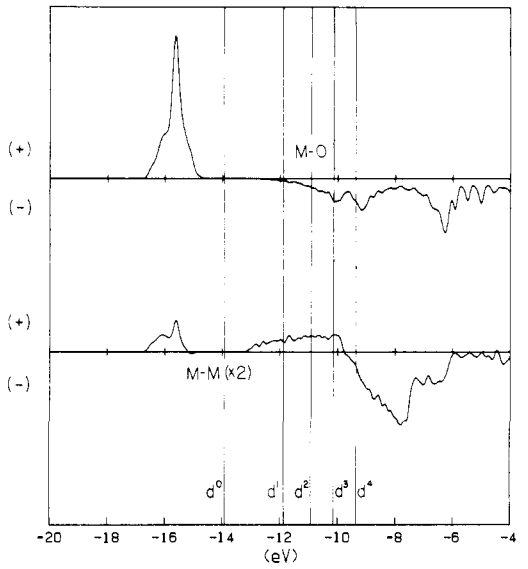

Figure 5. Crystal orbital overlap population (COOP) curves are shown for Ti–O bonds (top) and Ti–Ti bonds (bottom). The absolute scale is arbitrary, and the Ti–Ti curve is multiplied by 2 relative to the Ti–O curve.

Our results are quite similar to those obtained by previous workers. Comparison of d–d splittings at various symmetry points[10] in the Brillouin zone are within ≤10% of those reported by Neckel and co-workers from augmented plane wave calculations.[11a] This rather close correspondence is indicative of the extent to which the electronic structure of these compounds is controlled by symmetry constraints and the remarkable ability of the extended Hückel (EH) ansatz to reproduce the semiquantitative details of the *magnitudes* of such splittings. This result, as well as results obtained from many other metallic transition-metal systems,[12] leads us to conclude that the EH method may well be at its best in treating such systems.[13]

To more closely examine the bonding character of the rock-salt TiO crystal orbitals, we present the crystal orbital overlap population (COOP) curves[12b] of Figure 5. These curves indicate the bonding (or antibonding) nature of the crystal orbitals as a function of level energy. Where the curves are positive the orbitals are bonding, where negative they are antibonding. As shown in the top curve, the "bond strength" of the Ti–O linkages is optimal for a d^0 system and becomes gradually attenuated as the d manifold is occupied—particularly beyond the d^1 electron count. The

(10) Details will be provided upon request.

(11) (a) Neckel, A.; Rostt, P.; Eibler, R.; Weinberger, P.; Schwarz, K. *J. Phys. C* **1976**, *9*, 579. See also the calculation by: Mattheiss, L. F. *Phys. Rev. B* **1972**, *5*, 290. In none of these treatments is any mention made of the fact that TiO (and VO) were known to be highly defective structures. (b) Some cluster calculations were recently performed to model defects in TiO: Ivanovskii, A. L.; Gubanov, V. A.; Zainulin, Yu. G.; Kurmaev, E. Z.; Butsman, M. P.; Sborovskii, B. I. *J. Struct. Chem.* **1982**, *23*, 854. (c) Wahnsiedler, W. E. *J. Solid State Chem.* **1983**, *49*, 195. (d) Wimmer, E.; Schwarz, K.; Podlovcky, R.; Herzig, P.; Neckel, A. *J. Phys. Chem. Solids* **1982**, *43*, 439. (e) Huisman, L. M.; Carlsson, A. E.; Gelatt, C. D.; Ehrenreich, H. *Phys. Rev. B: Condens. Matter* **1980**, *15*, 991. (f) Erbudak, M.; Gubanov, V.; Kurmaev, E. *J. Phys. Chem. Solids* **1978**, *39*, 1157.

(12) See, for example: (a) Whangbo, M.-H.; Hoffmann, R. *J. Am. Chem. Soc.* **1978**, *100*, 6093. (b) Hughbanks, T.; Hoffmann, R. *Ibid.* **1983**, *10*, 1150–1162; (c) *Ibid.* **1983**, *105*, 3528–3537. (d) Whangbo, M.-H.; Foshee, M. J. *Inorg. Chem.* **1981**, *20*, 113–118.

(13) Woolley, R. G. Nouv. *J. Chim.* **1981**, *5*, 219. The conclusions of this work were apparently the result of reliance upon EH calculations where rather contracted single ζ d functions were used.

Ti–Ti COOP curve remains positive for electron counts up to just beyond d^3. The magnitude of the Ti–Ti overlap population is not very large, even for the optimal electron filling.

Overall, the overlap population data suggest that beyond a d^1 occupancy, metal–metal bonding is only moderately enhanced at the cost of filling orbitals with d–p π^* character as far as Ti–O bonding is concerned.

Levels at the bottom of the d block in rock-salt TiO have metal–metal bonding character and mix in no oxygen character at all. This is a symmetry-based result as can be seen by examination of **4**, where the symmetry of the lowest d bonding orbital

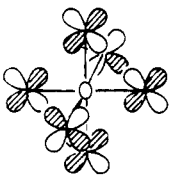

4

is made clearer by emphasizing the nodal characteristics of this crystal orbital about an oxygen atom. As it turns out, much of the lowest d band mixes in very little oxygen contribution, accounting for the fact that the overlap population between Ti and O is quite small for the levels at the bottom of the d block (see Figure 5).

Curiously, the rock-salt structure has long been considered a poor "candidate" for metal–metal bonding. The principle reason for this conclusion, however, is that in most compounds the anion radii (or the M–X bond length) are too large to allow the M–M distance to be very short.[14] The above treatment and the discussion that follows indicate that even where the metals *may* begin to get close—in oxides—the orbital topology of the structure still does not favor very strong metal–metal bonding. We will see that in the defect NbO and TiO structures this topology is very significantly altered.

Metal–Metal Bonding in NbO

If we do not explicitly consider the orbitals involved in metal–metal bonding in NbO, it is not apparent why such bonding ought to be much more extensive than in a rock-salt alternative. However, by removing an oxygen atom from a given site in a rock-salt structure, metal–metal bonding between the six metal atoms surrounding the nascent "vacancy" is enhanced as a result of two effects: (1) the metal orbitals formerly involved in M–O σ bonding now become involved, quite effectively, in M–M bonding, (2) the quasi-t_{2g} metal orbitals become considerably *more effective* in M–M bonding than in the rock-salt case. We now explore how these two effects arise.

When we remove from a rock-salt structure the complement of metal and oxygen atoms necessary to create the NbO structure, we must in turn consider the effects on the remaining metal and oxygen atoms. (The ejected atoms need not concern us since the idea of "removing" them in the first place is just a device for understanding the electronic structure of the "remaining" collection of atoms.) In presenting this discussion, we will consider every atom in the structure as situated with respect to a local coordinate system such that the z axis is perpendicular to the square plane of nearest-neighbor atoms and the x and y axes are directed at the neighbor atoms. Thus, for example, Nb "d_{xy}" orbitals are always surrounded by four O "p_z" orbitals giving rise to four d–pπ overlaps as illustrated in **5**. The net result of our choice of labeling is as follows: Nb xz,yz orbitals are directed at next nearest neighbor Nb's, xy orbitals are "in plane" orbitals that are not directed at Nb or O atoms, z^2 orbitals are directed at the oxide vacancies, x^2-y^2 orbitals are involved in Nb–O σ bonding, O x,y orbitals are involved in Nb–O σ bonding, O z orbitals are directed at Nb vacancies. We now turn to the explicit results of removing

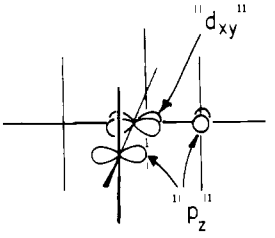

5

the Nb and O atoms from the rock-salt structure in "creating" NbO.

The effect upon the oxide ions in the structure is rather straightforward and is outlined schematically in **6**. Quite simply,

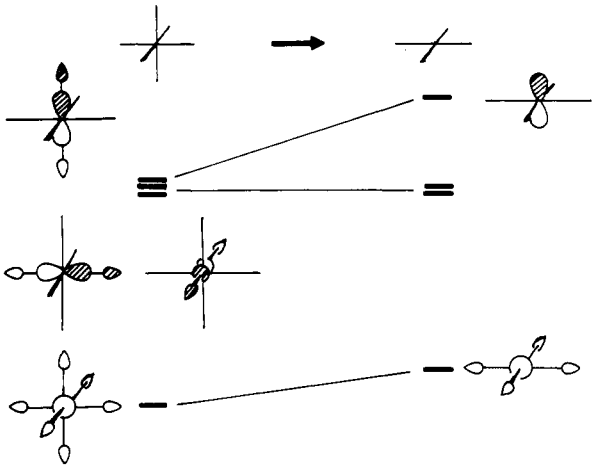

6

the p_z and to a lesser extent the s orbitals are destabilized by a loss of M–O σ bonding interaction. This state of affairs is one of the prime reasons why the NbO structure is "surprising"; four-coordinate oxygen is usually tetrahedral or nearly so. Clearly, if the oxygen p_z orbital can be stabilized by Nb d orbitals by π interactions this would provide some compensation for the loss of σ bonding. We will return to this factor below.

Considering now the effect of removing trans oxygens from each hitherto octahedral Nb, we expect a simple square-planar level diagram to emerge—as in **7**. The most important feature of **7**

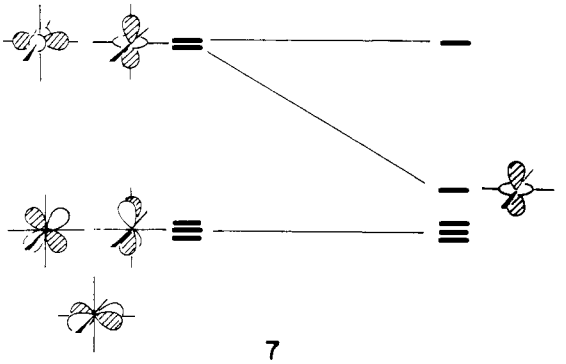

7

is the stabilization of the z^2 orbital upon the creation of the oxide vacancies. What is not evident at this junction is why a formally d^3 system should be appreciably stabilized by providing an additional low-lying d orbital. Indeed, three such orbitals were already available and, considering the rock-salt results of Figures 4 and 5, were metal–metal bonding in character (if only moderately so). The presence of this low-lying orbital is, however, crucial for our discussion.

A significant first step in understanding the enhanced metal–metal bonding in NbO comes in evaluating the overlap integrals between d orbitals on adjacent metal centers. As shown in Figure 3a, each Nb atom resides at the shared corners of octahedra in a cuboctahedral net. Focusing upon an edge of one of these

(14) Corbett, J. D. *J. Solid State Chem.* **1981**, *37*, 335 and references therein.

Table II. Some Relevant d–d Overlaps

type	angular decomposition	calcd value
$S_\sigma = \langle z^2\|z^2\rangle_{0°}$	S_σ	0.080
$S_\pi = \langle xz\|xz\rangle_{0°}$	S_π	0.080
$S_\delta = \langle xy\|xy\rangle_{0°}$	S_δ	0.019
$\langle z^2\|z^2\rangle$	$^1/_{16}S_\sigma + {}^{12}/_{16}S_\pi + {}^3/_{16}S_\delta$	0.069
$\langle xz\|xz\rangle$	$^3/_4S_\sigma + {}^1/_4S_\delta$	0.065
$\langle z^2\|xz\rangle$	$^3/_8S_\sigma - {}^3/_8S_\delta$	0.013
$\langle yz\|yz\rangle$	$^1/_2S_\pi + {}^1/_2S_\delta$	0.049
$\langle yz\|xy\rangle$	$^1/_2S_\pi - {}^1/_2S_\delta$	0.031

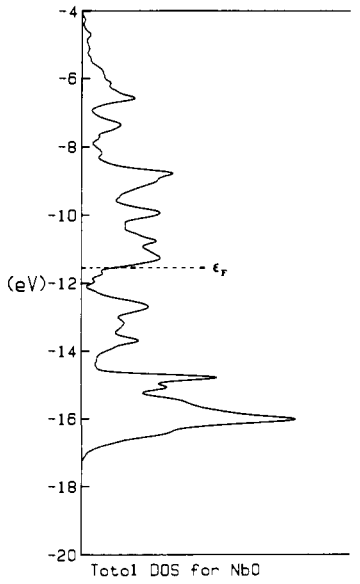

Figure 6. Total DOS for NbO. The Fermi level for NbO is at the d^3 line.

octahedra, we have tabulated in Table II the pairwise overlaps of d orbitals that belong to the atoms connected by that edge. The pairs tabulated are illustrated pictorially in **8**. Included in the

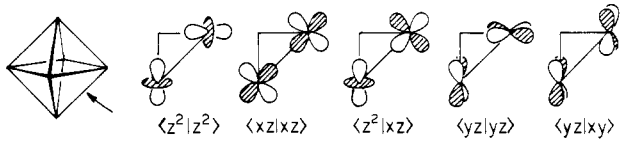

8

table are the angular overlap[15] decompositions of each overlap integral and the values calculated for each pair as well as that calculated for the basic (σ,π,δ) overlaps.

Table II contains a few surprises. First, we find that π overlaps are calculated to be as large as σ overlaps. While we may find this thought intuitively repellent, recall that metal–metal σ bonds typically include a fair amount of s and p hybridization and so are still "stronger" than π bonds. One should also recall that dπ orbitals more effectively extend into the region between atoms than pπ orbitals and hence experience with pσ and pπ overlaps may mislead. The second, more important, surprise of Table II is the large overlap between z^2-type orbitals ($\langle z^2|z^2\rangle$). The calculated value is in fact slightly larger than the seemingly dominant $\langle xz|xz\rangle$ contribution which couples the t_{2g} type orbitals on adjacent metal centers. The angular overlap decomposition of these two d–d overlaps reveals that they are so nearly equal precisely because the d–dπ and d–dσ overlaps are essentially equal. It is also notable that the z^2-type orbital on each metal is coupled effectively to *eight* nearest-neighbor metals via $\langle z^2|z^2\rangle$ overlaps. This is in contrast to the situation for t_{2g}-type orbitals, which overlap most effectively

(15) Smith, W.; Clack, D. W. *Rev. Roum. Chim.* **1975**, 9–10, 1243.

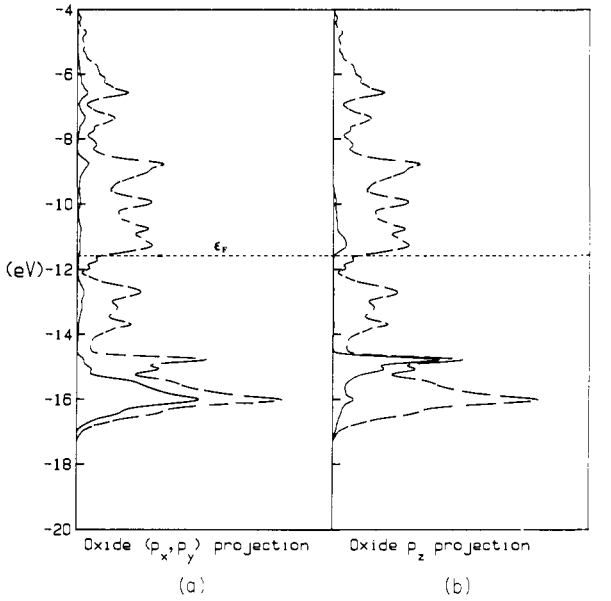

Figure 7. Oxide p contributions are projected: (a) the x,y contribution, (b) the z contribution. Note that the Fermi level lies just below the "upper peak" in (b). The total DOS is included for reference.

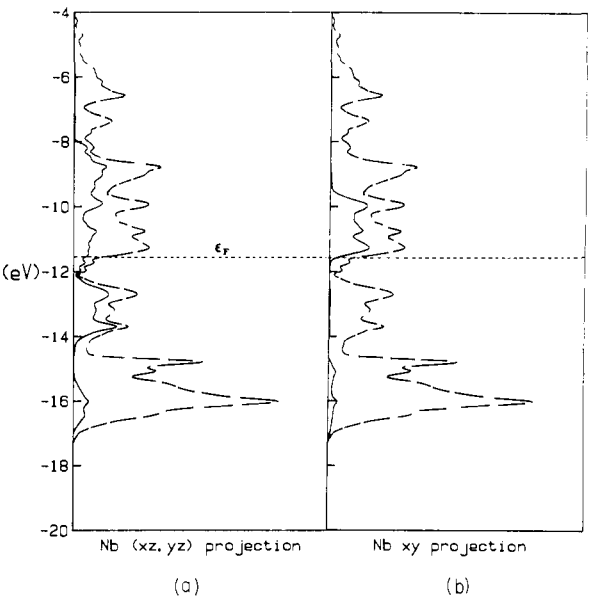

Figure 8. Nb contributions are projected: (a) the xz,yz contribution, (b) the xy contribution. Note the Fermi level. The total DOS is included for reference.

with only *four* nearest neighbors (via $\langle xz|xz\rangle$ overlaps).

We now examine the DOS for NbO, shown in Figure 6. The energy range displayed includes the oxide p bands as well as Nb d bands. The large lower peak (at ~−16 eV) is quite similar to the O p peak found for the rock-salt structure (cf. Figure 4). The remainder of the DOS is, however, strikingly different from that for rock salt. Our results are quite comparable to those reported by Wahnsiedler[11c] and especially those of Wimmer et al.[11d] in recent treatments of NbO using the APW method. While the EH bandwidths are somewhat narrower (~80%) than those obtained using the APW method, the DOS pattern is strikingly similar. Our results are therefore compatible with the XPS spectra reported by Erbudak et al.[11f]

Turning first to the oxide ion, in Figure 7 the oxygen p contributions are shown, p_x,p_y in (a) and p_z in (b). The p_x,p_y peak sits at low energy and is quite similar to the oxygen p peak for rock salt. The p_z peak is shifted up in energy and is responsible for the "shoulder" in the oxygen p part of the DOS. Generally, we find just what was expected: the pσ orbitals are stabilized more

than the pπ orbitals. Nevertheless, Figure 7b does show some significant stabilization of the oxygen p_z orbitals (as evidenced by the low-energy "tail" in the p_z contribution). Note that there is a small but clear peak in Figure 7b at higher energy, in fact just *above* the Fermi level.

Consider now the contribution to the DOS made by the Nb orbitals. The projected contributions of the *xz*, *yz*, and *xy* orbitals are shown in Figure 8. The *xy* contributions (Figure 8b) are understood in a straightforward fashion. By comparing Figures 7b and 8b, we see that the oxygen p_z and Nb *xy* distributions mirror each other; the peaks occur in the same energy ranges, and where the *xy* contributions are large the p_z contributions are small and vice versa. What is occurring, of course, is the formation of Nb–O d–pπ and d–pπ* bands. The π band, as expected, is predominantly O p_z and the π* band mostly Nb *xy*. Of particular importance is that the Fermi level in NbO lies *just below* the π* band. In an important sense, the NbO structure with a d^3 count is optimal if we wish to stabilize square-planar oxygen. For the *xz*,*yz* contribution (Figure 8a), the situation is more complicated but we note at this point that these orbitals are ca. one-half occupied at d^3 and form a rather wide set of bands.

Finally, we consider the contribution to the DOS made by the remaining d levels. The $x^2 - y^2$ orbitals, directed as they are at the surrounding oxides, make little contribution to the occupied bands except for some mixing into the lowest oxide bands during the formation of Nb–O σ bonding levels. The z^2 orbitals, however, are more interesting. As shown in Figure 9, the z^2 contribution to the occupied levels is significant. In fact, a detailed look at the band structure shows the lowest d band to have z^2 character with some s mixed into it. Just as in molecules, this s–d hybridization effectively stabilizes the z^2 orbitals by relieving z^2–oxygen antibonding interactions (as indicated in **9**). It also serves

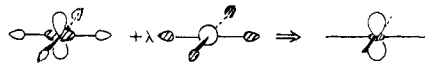

9

to enhance metal–metal bonding in a crucially important way. Because s–d and s–s overlaps are considerably larger than d–d overlap integrals, a small amount of hybridization can be important. Equation 1 indicates the decomposition of the overlap

$$\frac{1}{1+\lambda^2}\langle(z^2+\lambda s)|(z^2+\lambda s)\rangle = \frac{1}{1+\lambda^2}[\langle z^2|z^2\rangle + 2\lambda\langle z_2|s\rangle\tfrac{1}{4} + \lambda^2\langle s|s\rangle] \quad (1)$$

between two sd_{z^2} hybrids into a combination of fundamental d–d, s–d, and s–s overlaps. The hybrids are understood to be oriented as in **8**, this is responsible for the angular overlap factor of $^1/_4$ ($^1/_2(3\cos^2\theta - 1)$ where $j = \pi/4$) in the second term on the right-hand side of eq 1. Using a calculated value for the extent of hybridization at the bottom of the z^2 band ($\lambda \simeq 0.4$), we find that the effective overlap between these sz^2 hybrids is 0.115 to be compared with the value of 0.069 listed in Table II for the pure $\langle z^2|z^2\rangle$ case. Due to this enhanced effective overlap as well as to the fact that these orbitals are coupled to eight neighbors (as mentioned earlier), the in-phase combination of sz^2 hybrids is found at very low energy (~15.8 eV). This explains the absence of a gap between the formal Nb d bands and O p bands, in contrast to the situation we observed for the rock-salt structure (cf. Figure 3). In a nutshell, this arises simply because s–d mixing is prohibited by symmetry for octahedral coordination but allowed for square planar.

The results discussed up to this point are schematically summarized in Figure 10 where we present a simplified picture for the bonding in NbO. Occupied levels are shaded. Counting electrons using this picture is straightforward: the oxide levels are of course completely occupied; the z^2 and (*xz*,*yz*) orbitals are formally half occupied with the three d electrons per Nb; the *xy* orbitals are formally vacant because they have been pushed up by π interaction; the $x^2 - y^2$ orbital becomes a σ* orbital. Some

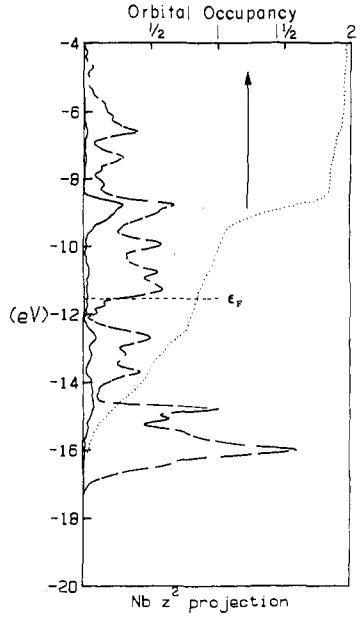

Figure 9. Nb z^2 contribution is projected. An integrated curve is given to indicate the extent to which the z^2 orbital is occupied, and the upper abscissa indicates the scale. The total DOS and Fermi level are also shown.

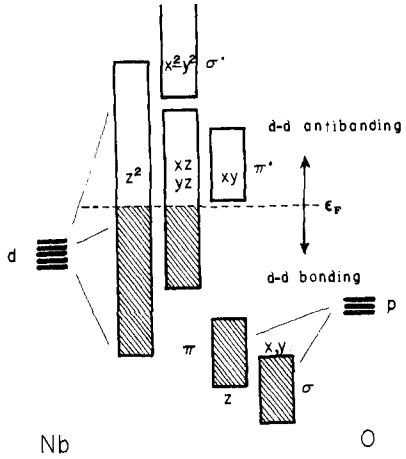

Figure 10. Schematic level diagram for NbO is shown. Occupied levels are shaded—note that a d^3 count is formally accounted for by the scheme, which implies a $(xz)^1(yz)^1(z^2)^1$ configuration.

of the details we have discussed above are depicted in this diagram as well.

The results we have presented so far make clear those factors that contribute to the stabilization of the NbO structure at d^3. The COOP curves for the Nb–O and Nb–Nb bonds nicely amplify this discussion. These are shown in Figure 11. Occupied levels for the observed d^3 case are shaded and alternative Fermi levels are indicated for the d^0, d^1, d^2, and d^4 cases by the vertical lines. These curves quite clearly imply that the optimal occupancy is indeed d^3; fewer electrons would not take full advantage of metal–metal bonding orbitals, and more would occupy Nb–O antibonding levels and, ultimately, Nb–Nb antibonding levels. The effect of occupying Nb–O π* levels can be clearly seen on moving from d^3 to d^4—although it appears a small compensating increase in Nb–Nb bonding would result. Of prime importance overall is the striking differences in metal–metal bonding between the rock salt and NbO structures (compare Figures 5 and 11).

Analogy to 6–12 Clusters

Earlier, we suggested that clusters such as $Nb_6Cl_{12}^{2+}$ provided a structural link with molecular chemistry[5,6] that is useful in understanding the NbO structure. The structure of such clusters is just what has already been shown as the NbO unit cell, structure

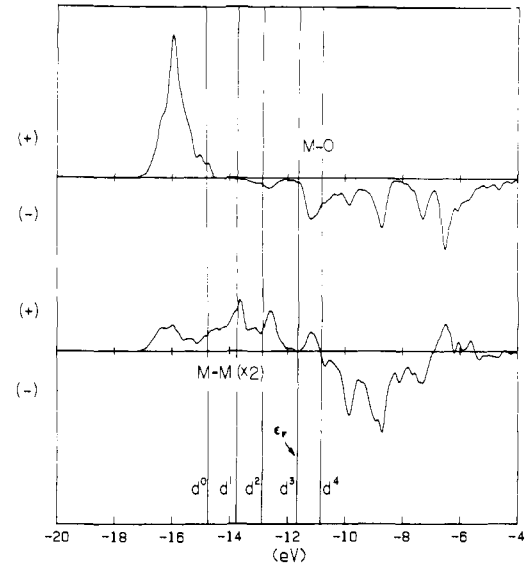

Figure 11. COOP curves for Nb–O bonds (top) and Nb–Nb bonds (bottom) in NbO. The Fermi level for NbO is at the d^3 line and additional lines indicate Fermi energies for alternative d electron counts. The absolute scale is arbitrary and the Nb–Nb curve is multiplied by 2 relative to the Nb–O curve.

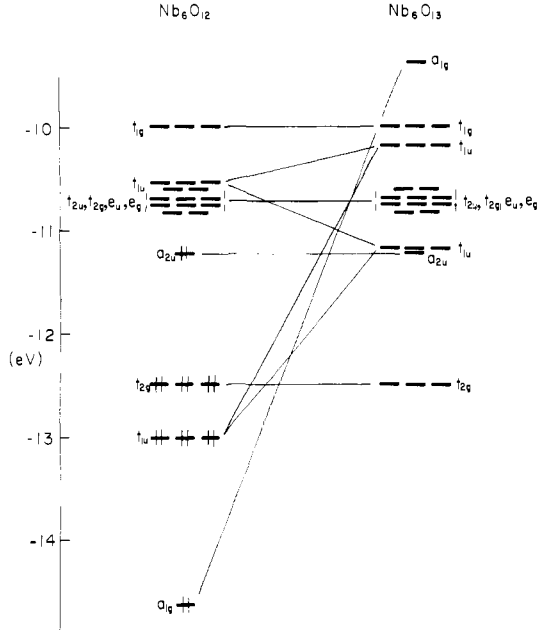

Figure 12. Level diagram for model Nb_6O_{12} and Nb_6O_{13} clusters. Occupancy shown for Nb_6O_{12} is appropriate for a $Nb_6O_{12}^{10-}$ species.

1. We now examine how far this viewpoint may be extended in approaching the actual electronic structure of these systems.

The electronic structure of 6–12 clusters has been the subject of a number of investigations, both experimental[16] and theoretical,[16c,17] and will not be discussed in much detail here. Instead we shall consider a model Nb_6O_{12} and Nb_6O_{13} calculation and

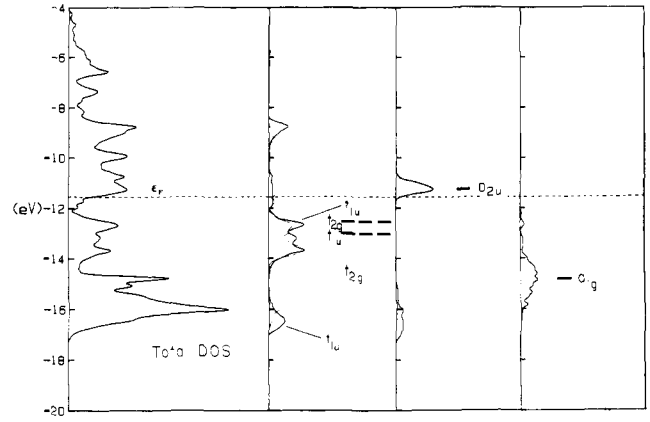

Figure 13. Orbital symmetry characteristics for NbO are displayed in these projections. The corresponding MO levels of Nb_6O_{12} are given in the appropriate panels for comparison. All the projections have been multiplied by 3 for clarity. See text for details.

look for features in the electronic structure (specifically, the metal-based levels) that may be transferable to the condensed NbO case. Figure 12 shows the orbital correlation diagram showing the effect of inserting an oxygen atom into the center of a Nb_6O_{12} cluster to produce Nb_6O_{13}. The dimensions of these systems were taken to be the same as in NbO itself: Nb–O = 2.107, Nb–Nb = 2.98 Å.

The results for Nb_6O_{12} are similar to those found in more complete earlier treatments[17c,e] and to results for Nb_6Cl_{12} systems using this method.[17f] This diagram indicates that there are seven levels that are unambiguously stabilized by metal–metal bonding (a_{1g}, t_{1u}, and t_{2g}). The a_{1g} level lies particularly low in energy because of d–s mixing (see above) and because, in contrast to the case for cluster compounds, there are no ligands capping the faces of the clusters. The addition of ligands would probably moderately destabilize this level and put it nearer to the t_{1u} and t_{2g} bonding levels. Just below the higher lying antibonding levels is an a_{2u} level, split off by $\sim^1/_2$ eV. In real systems, the a_{2u} level is calculated to be somewhat deeper in energy and can be approximately regarded as being overall nonbonding.[18] This scheme is consistent with the bulk of experimental data[16a,b,d,f] but cannot be said to be entirely settled in all details.[16c] Since these cluster compounds are not the overriding focus of this work, we will not discuss these issues further except to note that the total observed electron counts provide considerable support. M_6X_{12} systems are best known for $14e^-$, $15e^-$, and $16e^-$ systems (but see ref 16e)—the variable occupancy as well as EPR data[16a,f] suggesting a singly degenerate orbital capable of taking up 2 electrons. Clearly, the a_{2u} orbital fits this requirement.

What about Nb_6O_{13}, our "rock-salt analogue"? The result of the Nb_6O_{12} + O "reaction" is understandable on symmetry grounds. Since the central oxygen has $a_{1g}(s)$ and $t_{1u}(p)$ donor orbitals, the corresponding metal–metal bonding Nb_6O_{12} levels are destabilized upon addition of the central oxygen—illustrated in **10**. This loss of metal–metal bonding levels obviously parallels

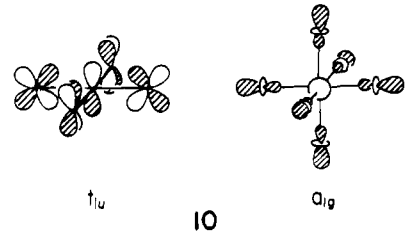

10

the analogous situation when oxygen atoms are added to NbO to give the rock-salt structure.

The relationship between Nb_6O_{12} and NbO can be demonstrated explicitly if we extract from the levels of NbO those with particular symmetry characteristics with respect to the O_h point symmetry at an oxygen vacancy site. That is, we can project from

(16) (a) Mackay, R. A.; Schneifer, R. F. *Inorg. Chem.* **1967**, *6*, 549. (b) Converse, J. G.; McCarley, R. E. *Ibid.* **1970**, *9*, 1361. (c) Robbins, D. J.; Thomson, A. J. *J. Chem. Soc. Dalton Trans.* **1972**, 2350. (d) Edwards, P. A.; McCarley, R. E.; Torgeson, D. R. *Inorg. Chem.* **1972**, *11*, 1185. (e) Corbett, J. D. *J. Am. Chem. Soc.* **1978**, *100*, 652. (f) Klendworth, D. D.; Walton, R. A. *Inorg. Chem.* **1981**, *20*, 1151–1155.

(17) (a) Cotton, F. A.; Haas, T. E. *Inorg. Chem.* **1964**, *3*, 10–17. (b) Robin, M. B.; Kuebler, N. A. *Ibid.* **1965**, *4*, 978. (c) Vovonovich, N. S.; Konol'kov, D. V. *J. Struct. Chem.* **1971**, *12*, 458, 613. (d) Muller, H. *Z. Phys. Chem. (Leipzig)* **1972**, *249*, 1. (e) Wirsich, J. *Theor. Chim. Acta* **1974**, *34*, 67. (f) Hughbanks, T., unpublished results.

(18) M_6X_{12} clusters generally are such that the inner octahedron of metals is considerably contracted from the faces of the ligand cuboctahedron and this acts to stabilize this level by enhancing metal–metal bonding relative to metal–ligand antibonding interactions.

the total DOS those parts that have a_{1g}, a_{2u}, t_{1g}, ..., etc. symmetry about the center of an octahedron of Nb atoms in NbO. In doing so we are doing nothing more than graphically presenting the results of Mulliken population analysis using symmetry-adapted linear combinations as a basis. Translational symmetry guarantees, of course, that all such O_h sites in the crystal are equivalent. In Figure 13, we show the results of such an analysis for NbO with levels of t_{2g}, t_{1u}, a_{2u}, and a_{1g} symmetry displayed. The total DOS appears at left for reference. The t_{2g} and t_{1u} projections are plotted together because of their considerable overlap in energy; also the t_{1u} part neglects any z^2-type contribution because this proves to be small in the occupied energy range. The a_{2u} projection has pure xy-type character (cf. Figure 8b), and the a_{1g} projection is a a_{1g} linear combination of z^2, s, and p orbitals obtained as the lowest MO from a molecular orbital calculation on a Nb_6 cluster. The energies of the molecular orbitals from our Nb_6O_{12} model are also shown with the corresponding projections (these are the same levels of Figure 12 discussed above).

When analyzed as in Figure 13, the occupied levels in NbO bear a striking resemblance to those in the 6–12 clusters. To be sure, the sharp MO energy levels are broadened, but the energy distribution of levels is quite similar in the cluster and solid. The correspondence between the a_{2u} MO level and the a_{2u} projection is remarkably close but not unexpected considering our identification of the xy-type levels as having d–pπ* character. The a_{2u} level is likewise the LUMO in $14e^-$ 6–12 systems; it has M–M bonding and M–O antibonding character **11**. Without recourse

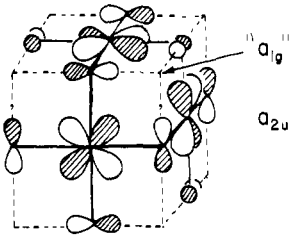

11

to the cluster analogy the t_{2g} contribution would be difficult to rationalize. Naively, we expected this to appear very much as in rock salt; certainly the considerably more peaked appearance is more reminiscent of the MO's of Nb_6O_{12}.

While the correspondence between the symmetry characteristics of the cluster molecular orbitals and the NbO crystal orbitals is indeed close, we note that we cannot use this correspondence for the purpose of electron counting because the Nb_6 octahedra in NbO are fused. The symmetry adapted basis used to construct Figure 13 is not independent, we can use such a basis only to investigate the symmetry characteristics of the crystal orbitals.

The correspondence between NbO and the 6–12 cluster does suggest an interesting possibility. Can NbO be "reduced" (say, by intercalation) by filling the a_{2u}-like xy-type levels above the Fermi level? Such a reduction would of course entail a formal Nb oxidation state considerably lower (>2) than actually found in the molecular analogues (2.33–2.67), but the formal orbital symmetry correspondence suggests the plausibility of adding electrons to the system. Since this would involve the filling of levels with d–pπ* character, stabilization of the oxygen p_z orbitals by some means beyond Nb–O π bonding should be more promising than merely "adding" electrons by substitution of Nb with, say, Mo. Intercalation with perhaps Al^{3+} or In^{3+} seemed reasonable to us but failed to perturb the a_{2u} levels to any appreciable extent in calculations on $AlNb_6O_6$ and $InNb_6O_6$. A crystal orbital of a_{2u} symmetry about an oxygen vacancy (i.e., the center of the Nb_6X_{12}-like octahedron) is constrained necessarily to have a_{1g} symmetry *about a site of intercalation* (i.e., the center of an oxide octahedron). This can be seen by inspection of **11**. Therefore only the Al (or In) s orbital interacts with the a_{2u} NbO crystal orbital. However, the oxygen and niobium overlaps with the s orbital have opposite signs and combine to give a quite small net overlap.

TiO

Because of the more complex and lower symmetry of the TiO structure, the kind of orbitally detailed description we have given for the electronic structure of NbO is more than we can give. Our strategy shall be instead to look for similarities to the NbO system and to try and understand what the differences are as well. Indeed there are two important experimental aspects in which the NbO and TiO systems differ: (a) the defect concentrations in the stoichiometric compounds differ, only one-sixth of the rock-salt atoms are missing in TiO vs. 1/4 in NbO; (b) the TiO system has long been known to exhibit marked nonstoichiometry[19-21,3] which is manifested differently on the metal-rich and oxygen-rich sides.[3a]

As mentioned earlier, nonstoichiometry on the O-rich side of TiO appears to be accommodated by intergrowth of TiO and $TiO_{1.25}$ at least for a low-temperature form with the reported composition $TiO_{1.19}$.[3a] The data on the metal-rich side indicates a filling up of the Ti defects until the composition $TiO_{0.84}$ is reached at which point the metal sublattice is virtually complete. An orthorhombic superstructure, however, accommodates the crystallographic data for composition in the range $TiO_{0.7}$–$TiO_{0.9}$. We will offer some comments on these aspects after presenting features of the TiO electronic structure.

The results we present for TiO will be those obtained from calculations using the Nb parameters used for NbO because we will wish to make energetic comparisons. Except for a slightly smaller d bandwidth and upward shift in the d levels relative to the oxide p bands, calculations using Ti parameters gave very similar results. Hereafter we shall not make any explicit distinction between TiO and NbO in the TiO structure. The M–O distance was maintained at that for NbO (2.107 Å). Further details are given in the Appendix.

We shall not attempt to deal with the details of the TiO electronic structure in terms of the AO's at each site in the crystals, instead we will go directly to consideration of the structure of the oxide vacancies and metal octahedra. While NbO represents a structure in which M_6O_{12} clusters may be considered as *fused* with adjacent clusters on all faces, in TiO this fusion occurs in only one dimension. Thus, chains such as shown in **12** may be rec-

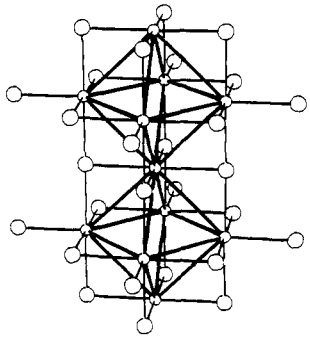

12

ognized in the structure. The fusion of such chains to construct the full TiO structure is complicated but does not significantly alter the coordination environment of the metal atoms in the chain, and hence **12** proves to be a good model for the metal–metal bonding in TiO. This is merely because this chain contains all M–M "bonds" that are not bridged by two oxides (i.e., all bonds that are not as they are in the rock-salt structure). For expository economy, however, we shall analyze our calculations from a viewpoint that emphasizes the connection with NbO and the M_6X_{12} clusters. See the paper of Huisman et al.[11e] for an alternative approach.

(19) Ehrlich, Pl. *Z. Anorg. Allg. Chem.* **1941**, *247*, 53.
(20) Andersson, S.; Collen, B.; Kuylenstierna, U.; Magneli, A. *Acta Chem. Scand.* **1957**, *11*, 1641.
(21) Hansen, M. "Constitution of Binary Alloys", 2nd ed.; McGraw-Hill: New York, 1958; p 1068.

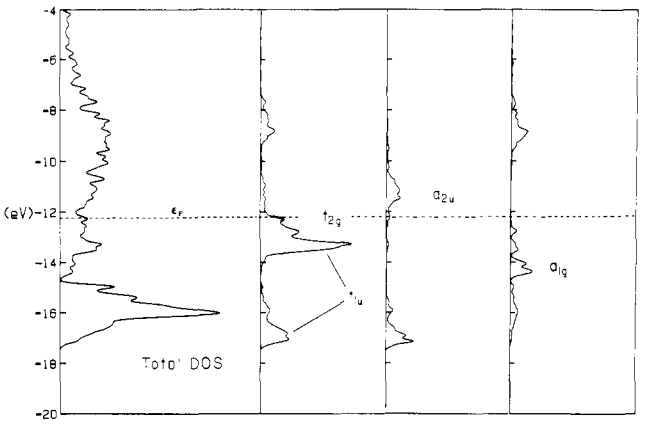

Figure 14. Total DOS and various projections for the TiO structure (Nb parameters used). The projections are scaled relative to the total DOS by multiplying by 5.

Figure 14 shows the total DOS for the TiO structure along with some key projected contributions. This figure is entirely analogous to Figure 13, and our earlier comments explaining that figure apply to Figure 14 as well. For the most part the two cases are quite similar. The a_{2u} and a_{1g} components are certainly not as "clean" as for the NbO case; this is a result of the lower site symmetry actually found at an oxide vacancy in TiO. Additional calculations on a Ti_5O_{12} model chain (**12**) show the a_1 levels for that system mirror the behavior of the a_{1g} projection shown in Figure 14. The a_{2u} component extends over a larger energy range because in TiO the *xy*-type d orbitals overlap with orbitals on two neighboring Ti atoms whereas in the NbO system they are directed only at Nb vacancies. Note also that the t_{2g} levels are no longer peaked about the energy of the Nb_6O_{12} t_{2g} level as was the case in NbO (cf. Figure 13). These are minor variations, however; the Ti octahedra in TiO are quite similar to those in NbO and in the M_6X_{12} clusters.

The total DOS for TiO certainly shows fewer d levels to have been stabilized (relative to rock salt) than in NbO. This is expected on the basis of fewer oxide vacancies in TiO. In consonance with this fact is the much less distinct splitting of the entire d block as compared with NbO. Electronically as well as structurally, TiO is a compromise between NbO and rock salt.

This compromise is nicely underscored by the behavior of the COOP curves for the TiO structure. There are a multitude of symmetry inequivalent bonds in TiO, but in practice these may be divided into three categories: (i) M–O, (ii) M–M bridged by two oxygens, (iii) M–M bridged by one oxygen. The rock-salt structure contains M–M bonds of type ii only, and NbO contains those of type iii only. It turns out that TiO has exactly the same number of type ii and iii. The COOP curves of Figure 15 show these "bonds" bear more than merely a structural resemblance to the rock salt and NbO analogues. At the top of the figure is an average curve for all the M–O bonds in the structure, at the bottom are shown curves for the singly and doubly bridged M–M bonds. A comparison with the type ii analogues of rock salt (cf. Figure 5) and the type iii analogues of NbO (cf. Figure 11) is telling. The potential metal–metal bonding between transition metals is greatly influenced by the presence of bridging main-group atoms. This amplifies earlier results for molecules[22] and extended systems.[12c] Whether a system will take advantage of such potential opportunities for metal–metal bonding depends upon electron count and geometric constraints.[14]

If we subdivide the M–O bonds into categories according to their characteristics with respect to the local coordination of the atom pairs making up the bonds, some interesting results emerge. Among these results the most surprising is the trend in overlap populations which one might have predicted on the basis of

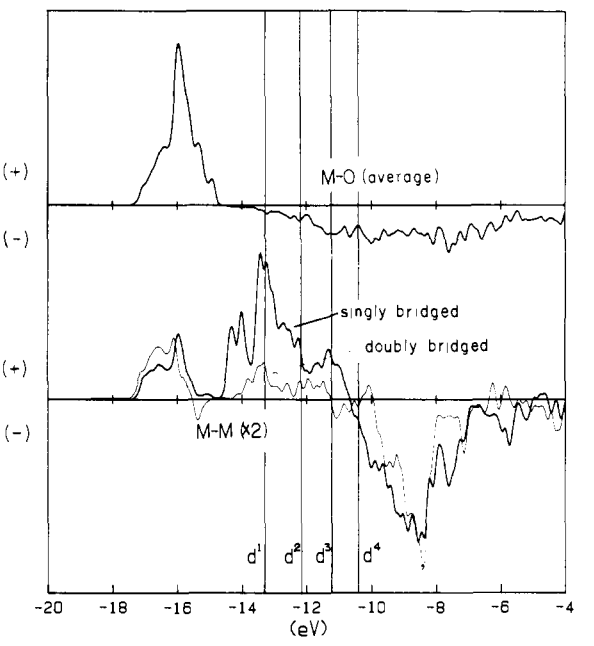

Figure 15. COOP curves are shown for M–O bonds (top) and M–M bonds (bottom) for the TiO structure. The top curve is the mean for all M–O bonds; the bottom curves are averages over the bond type indicated. The M–M bonds are scaled by a factor of 2.

"trans-influence" expectations.[23] The three categories are pictorially represented in **13**: M–O bonds that are between

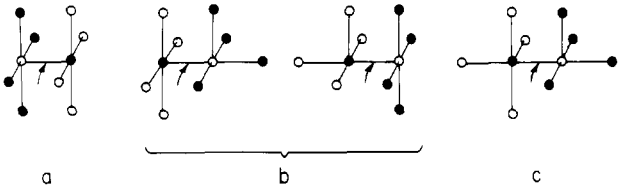

13

square-pyramidal metal and oxygen centers are (a) apical–apical, (b) apical–basal, and (c) basal–basal with reference to the square pyramids of the metal and oxygen atoms. Simple applications of trans-influence concepts would lead to us expect an ordering of overlap populations (bond strengths) of (a) > (b) > (c), in fact the calculated overlap population trend is just the opposite: (c) > (b) > (a). The implicitly ignored metal–metal interactions clearly exert a significant trans influence!

It should be noted that the "strongest" of the M–O bonds are those to the square-planar sites, be they square-planar metals or oxygens. As in NbO, M–O π bonding is implicated. A more careful analysis of the metal d orbitals that may participate in M–O bonding supports this implication. In this case we focus upon the d combination on the four metal atoms surrounding each square-planar oxygen which overlaps with the pπ orbital (i.e., has a_{1g} symmetry about the locally D_{4h} site in which the square-planar oxygens reside)—see **14**. As in NbO, the π^* levels are virtually empty.

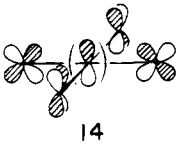

14

Once again, we may wish to consider the possibility of "adding" or "subtracting" electrons from the system; in other words, what are our chances of finding systems of the same or similar structure

(22) Shaik, S.; Hoffmann, R.; Fisel, C. R.; Summerville, R. H. *J. Am. Chem. Soc.* **1980**, *102*, 4555.

(23) See, for example, the short metal–apical oxygen bonds in fresnoite and stibivanite: (a) Moore, P. B.; Louisnathan, J. *Science (Washington, D.C.)* **1967**, *156*, 1361. (b) Kaiman, S.; Harris, D. C.; Dutrizac, J. E. *Can. Mineral.* **1980**, *18*, 329. Szymanski, J. T. *Ibid.* **1980**, *18*, 333.

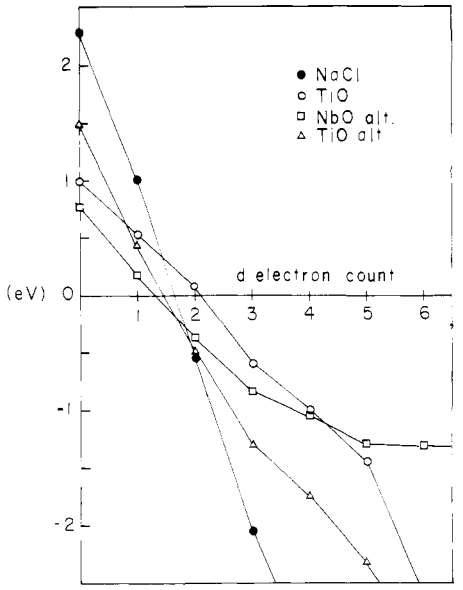

Figure 16. Relative energy curves for the structures indicated vs. NbO as a function of the formal d-electron count. For a given electron count the curve taking the greatest value indicates the most stable structure—NbO is given by the base line.

with a different electron count? In one sense, the fact that the TiO system exhibits such a rich chemistry of nonstoichiometric phases is an answer to this question. Indeed, the low-temperature modification of the material $TiO_{0.84}$ contains a virtually perfect metal sublattice[3a,24] and may be regarded as approximately $Ti^{IV}_{1/5}$ (TiO). Although the defect ordering may be somewhat altered, metal octahedra are still found to accept extra electrons, while the extra metals can be considered as in IV oxidation state by virtue of their six-coordination (i.e., they are rock salt like). The ability of TiO to accept additional electrons is reasonable in view of Figure 15 where levels above d^2 are metal–metal bonding though they are increasingly metal–oxygen antibonding. It is also interesting that $TiO_{1.19}$ has been identified as an intergrowth of TiO and $TiO_{1.25}$—perhaps indicating that the TiO structure "resists" the removal of the strongly bonding electrons below the d^2 level. Overall, the nonstoichiometry exhibited by the TiO system should be regarded as difficult to explain and our comments on this subject as speculative. We feel, however, an investigation of possible ternary systems in which the Ti vacancies of TiO would be filled by a main group cation would be worthwhile if only to discover whether the TiO structure would remain otherwise intact.

Energetics: NbO and TiO vs. Alternative Structures

Up to this point we have focused our attention upon the electronic structure of NbO and TiO and contrasted our results for these systems with those for a rock-salt alternative. We have ignored, thus far, any actual energetic comparisons. There are a number of reasons for this and prominent among them is that our method of calculation is not generally reliable in making energetic comparisons between structures with different coordination numbers. We shall find, however, some of the trends in the relative total energies are quite compelling despite the method's limitations. Subsequently, we shall make comparisons between NbO and other four-connected net structures. In these cases the EH method should be on firmer foundations since the energies will depend upon changes in the angular distribution of nearest neighbors in the structures being compared.

We have performed calculations on five structures discussed so far in this paper to obtain the total energies for these structures as a function of valence electron count. Results of these calculations are displayed graphically in Figure 16. Nearest-neighbor Nb–O distances were constrained to be 2.107 Å, and Nb parameters were used throughout. We have plotted the difference in total energy between that for the NbO structure and four alternatives to yield the four curves shown. Thus, the total energy of NbO constitutes the base line in the figure. Where a curve is above (below) this line the corresponding structure is calculated to be more (less) stable than NbO.

For any electron count greater than d^2, we calculate the NbO structure to be most stable. On the other hand, for a d^0 compound, NbO is less stable than any alternative, and the rock-salt structure is found to be favored by a considerable margin over any other structure. Remarkably, the TiO structure is found to be most stable in a fairly narrow range of electron counts around d^2 while for a d^1 count rock salt is the most stable. ScO is reported to have the rock-salt structure.[25] The most evident characteristic of the plot is the rapidity with which every alternative to NbO becomes increasingly unstable as the d electron count increases from zero. This is clearly symptomatic of the fact that NbO possesses so many low-lying metal–metal bonding levels. The filling of these levels is enough to compensate for the fewer number of Nb–O bonds per formula unit. The NbO and TiO alternative structures discussed with reference to the ionic model are seen in Figure 16 never to be the preferred structures. However, the ionic model and our EH results are in nearly complete agreement as to the relative ordering of structures *when we use d^0 results*, the only difference being the inversion of TiO and the NbO alternative. This is striking in view of the very different physical pictures that underlie the two models.

Despite the fact that the EH method does not generally serve as a good model for comparing structures with atoms possessing different coordination numbers, the above results are quite good. Why? Certain quantitative aspects are probably fortuitous (e.g., TiO vs. NbO at d^2), but our more extensive analysis in the earlier sections of this paper indicates that the overall trends of Figure 16 could not have come out differently. Clearly the downward slopes of the curves are inevitable as is the much greater slope of the NaCl curve vs. the TiO curve. Our discussion of the advantage (topologically) of having metal octahedra such as those in M_6X_{12} clusters helps make plausible the greater stability of NbO and TiO vs. our hypothetical alternatives. A more complete analysis of the electronic structure of these alternatives would certainly provide even more support but would take us too far afield. If we made allowances for the relaxation of the structures with d count, very little would likely change. Indeed NbO and TiO should probably be denser than assumed when we took M–O = constant throughout. This is a simple result of stronger metal–metal bonding and would act to reinforce the trends of Figure 16.

Much of this paper has been concerned with drawing a distinction between NbO and rock salt. Given that NbO is in fact a four-connected net, we may ask why this compound chooses the structure that it does within the set of possible four-connected structures.[27] To address this question, we should restrict ourselves to systems that meet some rather restrictive but reasonable constraints: (i) the nets should be *alternant* (i.e., all atoms are linked to atoms of the opposite variety); (ii) all links within a net must be the same length; (iii) the net must not constrain M–M contacts to be "unreasonably" close. Of nets that meet these constraints, we considered three to be most reasonable: (a) sphalerite, (b) PdO, (c) PbO; shown in **15** below.[2] The list is hardly exhaustive and there are a few alternatives that are omitted which might seem equally reasonable. One is the zincite (wurtzite) structure. This hexagonal analogue of sphalerite would certainly behave so much like sphalerite, energetically, there seems little point in including it. Another alternative might be an anti-PbO structure, which is indeed found for compounds like FeS and FeSe.[26] This was rejected because it violated restriction iii above.

(24) Eyring, L.; Tai, L.-T. "Treatise on Solid State Chemistry"; Hannay, H. B., Ed.; Plenum Press: New York, 1976; Vol. 3, p 167.

(25) No complete structure determination has, to our knowledge, been performed, however.

(26) (a) Evans, H. T.; Berner, R. A.; Milton, C. *Spec. Pap.—Geol. Soc. Am.* **1963**, *No. 73*, 147; *Geol. Surv. Prof. Pap. (U. S.)* **1964**, *No. 475-D*, 64. (b) Hägg, G.; Kindstrom, A.-L. *Z. Phys. Chem. (Wiesbaden)* **1933**, *B22*, 453.

(27) Wells, A. F. "Three Dimensional Nets and Polyhedra"; Wiley: New York, 1977; Chapter 9.

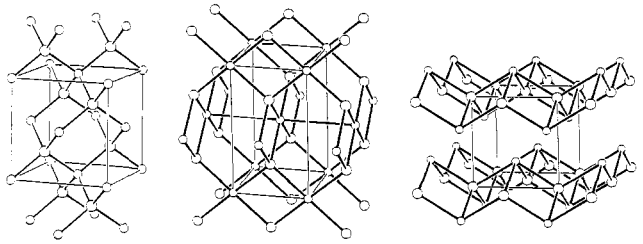

15

Each of these structures seem plausible as potential alternatives for NbO. The oxygen coordination is advantageous in all structures; in sphalerite the oxygens are in perfect tetrahedral coordination, and in the other two structures the tetrahedra are distorted. The PdO and especially the PbO structure would seem to offer possible enhanced metal–metal bonding though all metal–metal distances in the sphalerite structure are geometrically constrained to be rather long. It is particularly interesting to compare the PdO structure with the NbO structure. Both have metals in square-planar coordination with PdO enjoying the clear advantage of tetrahedral oxygen coordination.

Figure 17 shows the total energy curves that result from calculations on the structures. These curves have the same meaning as those of Figure 16; i.e., where the curves lie below the base line, NbO is calculated to be more stable than the corresponding structure—where the curves lie above the base line, the opposite is true. Two curves are plotted for the PdO structure in which the M–O–M angle α at the oxygens bridging adjacent metals has been varied: the "observed" structure in which $\alpha = 98°$ and a "contracted" geometry in which $\alpha = 90°$. As before, the M–O distance was maintained at 2.107 Å and Nb parameters were used throughout.

A particularly satisfying result of these calculations is the fact that all curves show a minimum at the d^3 electron count. This serves to reinforce our earlier discussion which indicates this electron count is optimal for stabilizing the NbO structure. The magnitude of the relative stabilization of the NbO structure is quite large: ≥1 eV relative to even the contracted PdO structure. The contraction allows a closer approach of the metal atoms than in the observed structure and hence somewhat better metal–metal bonding. Nevertheless, this contraction does not provide nearly enough stabilization to overcome the advantage enjoyed by the NbO structure at the d^3 count. The sphalerite structure is favored for d^0 and d^{10} electron counts—a result that clearly agrees with intuitive expectations and, for d^{10} counts, the experimental situation as well.[28]

Since the calculations on which Figure 17 are based only roughly correspond to any actual d^9 system, the sphalerite and PdO structures must be considered as close for that electron count. CuO[30] and AgO adopt the tenorite structure, which can be seen as a distorted PdO variant.

In accord with the observed structural data is the situation at d^8, the PdO structure is favored. In fact, the observed PdO structure becomes more stable than the contracted structure as the d count moves from six to eight. As the square-planar metals approach the "classical" d^8 configuration, the orbitals otherwise available for metal–metal bonding are filled and the metals move apart to avoid closed-shell repulsions.[29] Separate calculations on PdO using Pd parameters and the observed Pd–O distance were performed, and the structure was optimized with respect to variation of α. The optimal angle was found to be 95° (exptl: $\alpha = 98°$) and the calculated energy minimum was only ~ 0.5 kcal below the 98° geometry (i.e., the bending distortion was found to be rather soft). Given that Pd is considerably smaller than Nb, metal–metal interactions were of little importance in determining

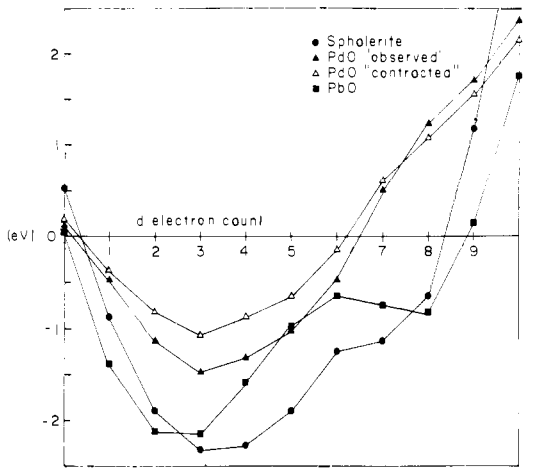

Figure 17. Relative energy curves for four-connected structures vs. NbO as a function of the formal metal d-electron count. The curves are interpreted as in Figure 16.

the optimal angle. Rather, the conventional view[2] that this angle is a trade-off between the tendency of Pd to be square planar ($\alpha = 90°$) and oxygen to be tetrahedral ($\alpha = 109.5°$) is quite appropriate.

Comparison of NbO and PdO indicates the importance of careful consideration of the overall orbital topology that a structure imposes. Consideration of the nearest-neighbor geometry is reasonable for PdO where metal–metal interactions are relatively small. In a niobium–oxygen system, the Nb/O size ratio forces us to consider the potential for metal–metal bonding that each structure allows. The metal–metal interactions enabled by the "NbO net" are clearly advantageous for a d^3 compound. In the PdO arrangement, only *two* next-nearest-neighbor metals can form unbridged metal–metal bonds (see **15b**) compared to the *eight* singly bridged contacts in NbO.

Finally we note that the PbO structure never appears as reasonable for any d count. However, we did not seek to optimize the structure with respect to the greater number of degrees of freedom possible for this structure even with the M–O bond length fixed. The structure was determined by taking the angles about the oxygen atoms equal to those in PbO[28] and the nearest M–M distance between layers shown in **15c** was taken to be 2.98 Å, as in NbO. The structure was found to be disfavored to such a large extent for all electron counts that it is unlikely that attempts to stabilize the structure by "relaxation" of geometrical parameters would alter this state of affairs.

Summary and Conclusions

Let us recapitulate the findings of this study that relate directly to the systems examined. Both the NbO and TiO structures are a natural result of the presence of numerous metal–metal bonding levels as compared with any alternatives studied. The stabilization of square-planar oxygen ions, particularly in NbO, also plays an important role in stabilizing these structures. Concepts of bonding in these compounds that exploit the structural analogies with M_6X_{12} clusters[5,6] have been buttressed by our results. Clear analogies can be drawn between the electronic structures of these systems. One of the principal advantages of drawing such analogies is that we may utilize experience gained in one area to suggest possibilities for others. It was in this spirit that we discussed the possibility of intercalation in NbO and new ways of interpreting the nonstoichiometry characteristic of the TiO system.

What about more general conclusions? First, we might ask whether related systems can be expected to have rock-salt defect structures. VO, though not exhibiting the NbO structure, does have a high concentration of vacancies (~16%).[31a] No ordered

(28) See, for example: Pearson, W. B. "The Crystal Chemistry and Physics of Metals and Alloys"; Wiley: New York, 1972. Also see ref 2.
(29) The inclusion of higher lying s and p orbitals on the metals ameliorates this repulsion. In fact, we find the metal–metal interaction to be bonding.
(30) Åsbrink, S.; Norrby, L.-J. *Acta Crystallogr., Sect. B* **1970**, *B26*, 8.
(31) (a) Westman, S.; Nordmark, C. *Acta Chem. Scand.* **1960**, *14*, 465. (b) Early "ZrO" phases seem likely to have been badly contaminated: Zainulin, Yu. G.; Alyamovskii, S. I.; Shveikin, O. P.; Gel'd, P. V. *Izv. Akad. Nauk. SSSR, Neorg. Mater.* **1970**, *6*, 1356; *Inorg. Mater.* (*Engl. Transl.*) **1970**, *6*, 1140.

Table III. Parameters for EH Calculations

	orbital	H_{ii}, eV	ζ_1[b]	ζ_2[b]	c_1[a]	c_2[a]
Nb[38]	4d	−12.1	4.080	1.640	0.6401	0.5516
	5s	−10.1	1.89			
	5p	−6.86	1.85			
Ti[39]	3d	−10.81	4.55	1.60	0.4391	0.7397
	4s	−8.97	1.50			
	4p	−5.44	1.50			
Pd[40]	4d	−14.07	5.98	2.613	0.5265	0.6372
	5s	−9.57	2.19			
	5p	−3.43	2.15			
O	2s	−32.3	2.275			
	2p	−14.8	2.275			

[a] Coefficients used in double-ζ expansion. [b] Slater-type orbital exponents.

structure is known but short-range order cannot be ruled out. Why doesn't VO exhibit the NbO structure? Certainly one factor is the smaller size of V than Nb. This makes metal–metal bonding less important within the "geometric" constraints imposed by the M vs. O size ratio.[14] Unfortunately, no stable phase with stoichiometry $ZrO_{1.0}$ has been prepared.[31b] The TaO system has been repeatedly investigated and the safest assessment at this point is to say that TaO thin films indeed show defects in both the Ta and O sublattices of NaCl superstructures.[32] HfN is closely related to the NbO and TiO systems: the electronegativity differences and metal–nonmetal "radius ratios" should be similar. Interestingly, HfN is reported to have a vacancy concentration of 12.6% in both sublattices,[33] a situation that tempts one to postulate an ordered defect superstructure with cubic symmetry in which one-eighth of the atoms are missing. Many other systems of relevance have been studied but much of the crystallographic data is not of sufficient accuracy to unambiguously determine vacancy concentrations or superstructures. Also, nonstoichiometric phases are often the only systems studied.

There are clearly transition-metal oxides we have not considered for which the sort of treatment we have given does not apply. The oxides of Mn through Ni are not compounds that can be considered as reasonably treated by the simple "low spin", delocalized picture we have provided. Various problems including magnetic ground states ("high-spin" analogues) and interstitial defects must be considered in a broader theoretical framework[7,3a] that we have used.

This study allows us to draw conclusions of a different sort. For example, the overlap population data we present (the COOP curves) make it clear that long held ideas about metal–metal bonding[35] are largely incorrect. M–M distances are a poor guide to M–M bond strength when used uncritically.[36] These systems also show how lattice energy calculations for systems in which metal–metal interactions can play a role are of little relevance in deciding about the plausibility of a given structure. Such classical approaches to understanding crystal structure are best restricted to cases in which the atomic constituents of a crystal are more reasonably described as closed-shell ions—and even in these cases this kind of approach is hardly foolproof. Clearly, a detailed study of the orbital topology presented by a given crystal structure can provide invaluable insight into the structural chemistry of solids.

Acknowledgment. We thank the donors of the Petroleum Research Fund, administered by the American Chemical Society, for their partial support of this research and the National Science Foundation via NSF DMR 8019741.

Appendix

The extended Hückel method[37] was used for all band structure calculations as well as for MO calculations. Parameters appear in Table III.

Pd H_{ii}'s were obtained by averaging charge iteration[41] results of calculations on PdO and PdS—where the latter compound was assumed to adopt the PdO structure with Pd–S = 2.32 Å. Ti s and p exponents were somewhat contracted with respect to those used by earlier workers to facilitate the more rapid convergence of lattice sums in band calculations. Various test calculations on molecules indicated this change was of little consequence for consideration of frontier orbitals.

In all calculations on crystals, matrix elements were computed between atoms separated by less than 8.5 Å. k-space meshes employed in calculations were as follows: for rocksalt structures, 220 k points (fcc lattice); for NbO structure, 120 k points (sc lattice); for TiO structure, 37 k points (face-centered monoclinic lattice). Each of the k-point meshes are referred to the number of points computed in the irreducible wedge of the appropriate Brillouin zones. A supercell of six Nb and six O atoms was used to produce the projected DOS curves of Figure 11. Because a correspondingly enlarged unit cell for TiO would entail a prohibitively expensive calculation, a modified procedure was needed to obtain the curves of Figure 12. This procedure did not require the use of a supercell and will be described in detail in a future publication. All DOS curves were smoothed using Gaussian functions with a standard deviation of 0.05 eV. k-point meshes used for other systems were as follows: NbO alternative, 126 k points (tetragonal); TiO alternative, 37 k points (centered monoclinic); sphalerite, 220 k points (fcc); PdO, 126 k points (tetragonal); PbO, 75 k points (tetragonal).

Registry No. NbO, 12034-57-0; TiO, 12137-20-1.

(32) Khitrova, V. I.; Klechkovskaya, V. V.; Pinsker, Z. G. *Kristallografiya* **1976**, *21*, 937; **1979**, *24*, 939.
(33) Straumanis, M. E.; Faunce, C. A. *Z. Anorg. Allg. Chem.* **1967**, *353*, 329.
(34) Glasson, D. R.; Jayaweera, S. A. A. *J. Appl. Chem. Biotechnol.* **1968**, *18*, 65.
(35) Pauling, L. "Nature of the Chemical Bond", 3rd ed.; Cornell University Press: Ithaca, 1960.
(36) The conclusion is put forward from a very different perspective in: Simon, A. *Struct. Bonding (Berlin)* **1979**, *36*, 81.
(37) Hoffmann, R. *J. Chem. Phys.* **1963**, *39*, 1397.
(38) Summerville, R. H.; Hoffmann, R. *J. Am. Chem. Soc.* **1976**, *98*, 7240.
(39) Richardson, J. W.; Nieuwpoort, W. C.; Powell, R. R.; Edgell, W. F. *J. Chem. Phys.* **1962**, *36*, 1057.
(40) Basch, H.; Gray, H. B. *Theor. Chim. Acta* **1966**, *4*, 367.
(41) Baranovskii, V. I.; Nikolskii, A. B. *Teor. Eksp. Khim.* **1967**, *3*, 527.